



CHORUS

This is the accepted manuscript made available via CHORUS. The article has been published as:

Probing the phase transition in VO₂ using few-cycle 1.8 μm pulses

M. R. Bionta, V. Wanie, V. Gruson, J. Chaillou, N. Émond, D. Lepage, P. Lassonde, M. Chaker, and F. Légaré

Phys. Rev. B **97**, 125126 — Published 16 March 2018

DOI: [10.1103/PhysRevB.97.125126](https://doi.org/10.1103/PhysRevB.97.125126)

Probing the phase transition in VO₂ using few-cycle, 1.8 μm pulses

M. R. Bionta,^{1,*} V. Wanie,¹ V. Gruson,^{1,2} J. Chaillou,¹ N. Émond,¹ D. Lepage,¹ P. Lassonde,¹ M. Chaker,¹ and F. Légaré^{1,†}

¹*Centre Énergie Matériaux et Télécommunications, Institut National de la Recherche Scientifique, 1650 Boulevard Lionel-Boulet, Varennes, Quebec J3X1S2, Canada*

²*Department of Physics, The Ohio State University, 191 West Woodruff Avenue, Columbus, OH 43210, USA*

We observe a nearly instantaneous triggering of the phase transition in VO₂ using transient, time-resolved absorption techniques from few-cycle, infrared (1.8 μm) laser pulses. The results are in agreement with the Mott-Hubbard insulator model, characterized by electronic holon-doublon pair creation that initiates the insulator-to-metal phase transition within the material. The spectral resolution provided by this technique can be exploited to measure the chirp of the probe pulses. Effects from probing above and below the band gap of the material are also discussed.

I. INTRODUCTION

Photo-induced phase transitions in strongly correlated materials, such as in vanadium dioxide (VO₂), are an important direction of research in condensed matter physics with many potential applications¹. When heated to above 340 K, VO₂ undergoes an insulator-to-metal phase transition (IMT). This transition has been extensively studied since its discovery by Morin in 1959². In 1971, Roach and Balberg showed that this same phase transition could be quickly induced by the optical excitation of a pulsed laser³. This led to discrepancies in the understanding of the nature of the IMT due to the fast timescales involved in the phase transition after photoexcitation. When driven by optical excitation, the IMT can be described by Mott physics^{4,5}, and in this work we aim to better understand the triggering mechanisms behind the IMT when induced by few-cycle laser pulses.

The mechanisms of the phase transition in VO₂ is quite controversial and subject to much debate and discussion of the processes surrounding the transition^{1,6-9}. Difficulties in observing the IMT arise from the fast nature of the transition. Questions remain regarding how fast and what initiates the phase transition.

Two leading theories prevail concerning the mechanism driving the VO₂ transition. It is unclear if the transition is initiated due to the prompt creation of holes causing a collapse of the band gap, or because of a change in atomic structural arrangement. If electron correlations are responsible for the phase transition, as determined by Mott physics, then the transition should appear to be instantaneous. In this scenario, the electric field triggers the creation of holon-doublon pairs^{10,11} which leads to an instantaneously detectable transient monoclinic metallic state^{9,12}. This is followed by an increase in the electronic temperature, leading to the distortion of the crystalline structure and final rutile state^{6,13}. As the transient monoclinic metallic state would show a change in transmission for an optical probe, a transition driven

by Mott physics would appear as instantaneous. However, if solely structural distortions are responsible via Peierls mechanisms¹⁴, then a slower transition would be detected^{6,15}. In this case, the increase in electronic temperature comes first from energy absorbed by the photons, leading to the creation of phonon modes. These phonon modes direct atomic structural motion creating the detectable rutile metallic state. As this detectable state occurs after a change in the atomic structure, the timescale of a transition driven by Peierls mechanisms would be much slower than that of Mott physics.

In 2004, Cavalleri *et al.* established a time-domain relationship between structural and electronic effects in VO₂ and reported a bottleneck time of 80 fs in the time of transition⁶, thus challenging the theory of Mott physics. They attributed this delay to Peierls mechanisms in which case the IMT is induced by lattice temperature effects arising from a slow phonon-mode. This initiates a structural motion which causes a collapse in the band gap. However, Kübler *et al.*^{7,8} in 2007, followed by Wegkamp *et al.*⁹ in 2014, both disputed this theory with evidence of a quasi-instantaneous IMT with no sign of a structural bottleneck up to the temporal resolution of their exciting laser systems (~40 fs and ~60 fs respectively). They concluded that the optical field creates photoexcited holes in the material, depleting the V 3d population, and thus collapsing the band gap without the need for a structural change. Thus, this creates an instantaneous IMT driven by the immediate creation of holes.

We confirm the results of Kübler *et al.*⁷ and Wegkamp *et al.*⁹ with a higher temporal resolution using 1.8 μm, 2.5 cycle (~15 fs) pulses, whose photon energy spans the band gap of the VO₂, showing that the transition time follows the duration of the pump pulses. This indicates an instantaneous response as described by Mott physics.

II. EXPERIMENTAL DETAILS

A 100 nm-thick epitaxial VO₂ sample was deposited onto a 532 μm, r-cut sapphire (Al₂O₃ (1102)) substrate using Reactive Pulsed Laser Deposition (RPLD) at the Laboratory of Micro and Nanofabrication (LMN),

* mina.bionta@emt.inrs.ca

† francois.legare@emt.inrs.ca

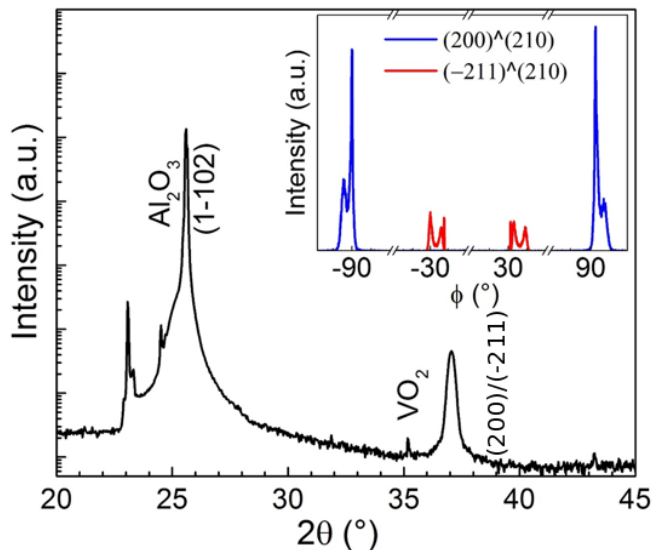


FIG. 1. XRD $\theta - 2\theta$ pattern of the VO₂ film deposited on a r-plane sapphire substrate. The inset shows the ϕ -scans of the off-axis (210) orientation tilted with respect to the (200) (blue curve) and (-211) (red curve) orientations respectively.

Canada¹⁶. The metallic vanadium target (99.95% purity, KJ Lesker) was ablated using a KrF laser ($\lambda = 248$ nm) at a fluence of 2 J cm^{-2} with a repetition rate of 10 Hz. During deposition, the oxygen pressure was kept at 20 mTorr and the substrate temperature was maintained at $550 \text{ }^\circ\text{C}$.

The crystalline quality of the film was evaluated using high resolution X-ray diffraction (XRD) measurements, shown in Fig. 1. The $\theta - 2\theta$ scan performed between 20° and 45° reveals the presence of peak at $2\theta \approx 37^\circ$, which is attributed to the (200) and (-211) orientations of monoclinic VO₂ (JCPDS #043-1051). The epitaxial growth of the film was confirmed by performing ϕ -scans of the VO₂ off-axis (210) peak at $2\theta = 42.27^\circ$ and at tilt angles $\chi = 28.09^\circ$ and $\chi = 67.80^\circ$ for (200) and (-211) orientation respectively.

The infrared (IR) transmission of the film was measured at 25 and $100 \text{ }^\circ\text{C}$ in a spectral range of $2.5\text{-}7 \mu\text{m}$ using a ThermoFisher Nicolet 6700 Fourier-Transform Infrared spectrometer (FTIR). The spectra were normalized to that of a reference spectrum taken through a bare sapphire substrate. The variation of the IR transmission of the VO₂ film across the insulator-to-metal transition ($\Delta T_{IR} = T_{25} - T_{100}$) at a wavelength of $2.5 \mu\text{m}$ is 68.13%. The band gap (E_g) of the sample was measured in 3 different places by measuring the coefficient of absorption in $(h\nu - E_g)^2$ with FTIR and found to be $E_g = 0.683 \pm 0.002 \text{ eV}$.

A standard four-point probe method was used to measure the electrical resistivity of the film at $25 \text{ }^\circ\text{C}$ (ρ_{25}) and $100 \text{ }^\circ\text{C}$ (ρ_{100}). The variation of the electrical resistivity of the VO₂ film across the IMT ($\Delta\rho = \log(\rho_{25}/\rho_{100})$) is 4.65 orders of magnitude. The bulk-like IMT characteristics of the epitaxially grown VO₂ film, attested by the

large values of ΔT_{IR} and $\Delta\rho$, confirm its high crystalline quality¹⁷.

A pump-probe setup, shown in Fig. 2(a), was constructed to measure the change in transmission through the VO₂ sample using few-cycle laser pulses centered at $1.8 \mu\text{m}$. The pulses are spectrally broadened through a hollow-core fiber setup¹⁸, then compressed using fused silica plates, and typically have a pulse duration of ~ 15 fs with a pump fluence on the order of tens of mJ cm^{-2} . The pulse duration and chirp were measured with a home built second harmonic generation Frequency Resolved Optical Gate (SHG-FROG)¹⁹, as shown in Fig. 2(b). The probe is separated from the pump using the surface reflection from a thin wedge. The low energy probe is transmitted through the sample at a variable delay from the pump, controlled with a Thorlabs 2825B DC stepper motor actuator. The spectra are recorded with an Oceans Optics NIR spectrometer or Spectral Products grating based slit monochromator with liquid nitrogen cooled HgCdTe detector. The energy of the pump pulse is controlled with a half-waveplate in combination with a Ge polarizer. The experiments were performed at room temperature of $20 \text{ }^\circ\text{C}$.

A fitting procedure was used to systematically define the frequency-resolved arrival time between the pump and the probe pulses. It also defines the frequency-resolved time of the transition as the size of the fitted step. This procedure is used for both the integrated spectrogram as well as the spectrally resolved measurements. The signal is given as

$$S(t, \omega) = \frac{S'(t, \omega) - R(\omega)}{R(\omega)} \quad (1)$$

where S' is the measured transmitted intensity of the probe, R is the reference defined as the average of probe intensity well before the pump arrives, t is the time delay between the pump and the probe pulses, and ω is the angular frequency of the laser field, or frequency range, investigated. This gives us a percentage change in transmission through the VO₂ sample.

This signal is then fit to an error function of the form:

$$S(t, \omega) = -a (\text{erf}(b(t - t_0(\omega)))) + 1) + d \cdot t \quad (2)$$

where t_0 defines the time overlap of the pump and probe pulses, i.e. the arrival time of the probe pulse at the sample. It is extracted from the inflection point, where the fitted equation changes sign in the second derivative. A linear term $d \cdot t$ is added to compensate for overall laser fluctuations, and this term is constrained to be very close to 0. The initiation time of the phase transition (TT) is related to b , with the FWHM of the transition given by $\sqrt{\log 2} \cdot b$. An example of this fitting can be seen in Fig. 2(d). In this case, the FWHM of the overall transition is determined to be 24 fs.

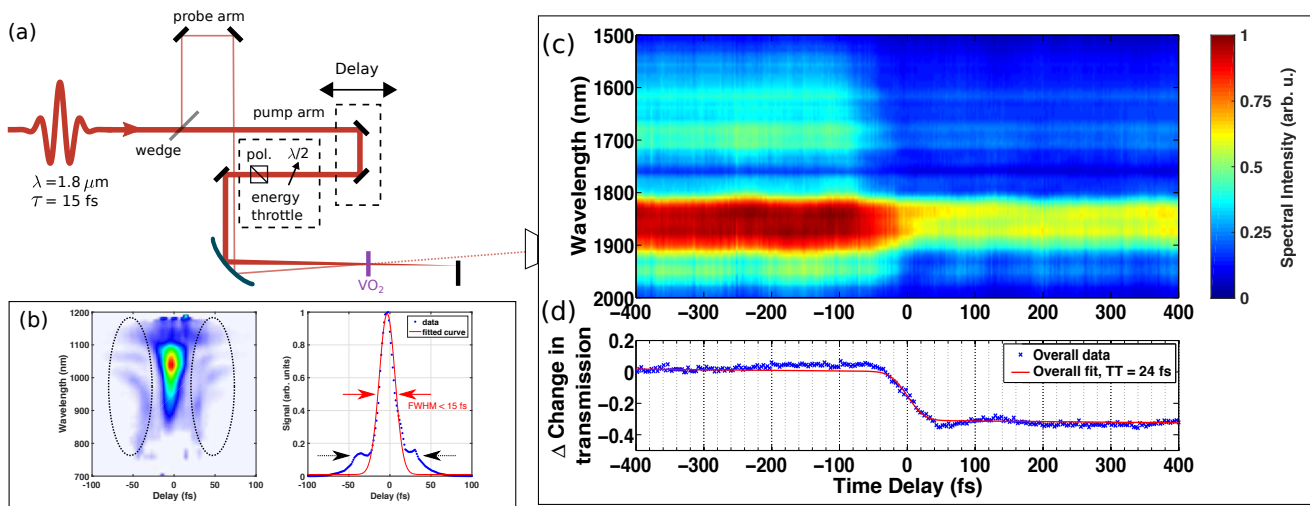


FIG. 2. (a) A pump-probe setup is constructed using few-cycle laser pulses centered at $1.8 \mu\text{m}$. The probe is separated from the pump using the surface reflection from a thin wedge. The energy of the pump is controlled using a half-waveplate, polarizer energy throttle. The low energy probe is transmitted through the sample at a variable delay from the pump and its transmitted spectra are recorded. The delay between the two pulses is controlled with a DC stepper motor actuator. (b) The SHG-FROG trace (left) and fitted pulse duration (right) of the compressed output of the fiber setup showing a < 15 fs pulse duration. The black circles and arrows show the uncompressed frequencies that make up the temporal pedestal of the pulse. (c) The spectrogram from the Ocean Optics spectrometer pumped to the maximum change in transmission with a laser fluence of 80 mJ cm^{-2} . (d) The recorded percent change in transmission with the transition time (TT) given by the fitting algorithm found to be 24 fs FWHM.

III. RESULTS AND DISCUSSION

The transition time reflects convolution of pulse durations of the pump and probe pulses. This is consistent with the theory of an electron driven holon-doublon hole pair creation in photoexcited VO_2 driving the phase transition. In a Mott-Hubbard phase transition, energy is deposited into the system from the laser via photoexcitation, causing an electron to hop from one site to another creating a electron hole, or holon, and a doubly occupied site, doublon. This increases the electron temperature, which disperses into the system via phonon relaxation. The electron-lattice coupling stabilizes the metallic phase and the structural distortions of the phase transition to form the rutile metallic form.

Using our pulses of 15 fs, we are able to show a transition time that depends on the pulse duration of the probe pulse. In Fig. 2(d), we pump the 100 nm epitaxially grown VO_2 sample to saturation with 80 mJ cm^{-2} of energy fluence. Saturation is defined the maximum change in transmission reached for the sample such that pumping the sample with more energy does not increase the change in transmission. Here we see that the fast, 24 fs FWHM transition time is consistent with the convolution of the two Gaussian 15 fs pump and probe pulses, as well as the induced geometric smearing caused by the spatial separation of the pump and probe. This is consistent with a nearly instantaneous response from the material.

The quickness of the observed phase transition can be explained as a Mott transition. In this case, we observe that the band gap closes within the pulse duration of the pump and probe initiating the phase transition.

III.1. Spectrally resolved results

Spectrally resolved measurements are in agreement with the pulse characterizations from the compressed output of the hollow-core fiber¹⁸. While the pulses are indeed few-cycle and short, they rest on a long, uncompressed pedestal as indicated by the black arrows shown on the SHG-FROG trace of right panel of Fig. 2(b). We can further spectrally resolve the pulse compression with the SHG-FROG trace (Fig. 2(b) left panel or in ref. 18) which clearly show uncompressed wavelengths indicated by the black dashed circles on the FROG trace. This is confirmed by the spectrally resolved change in transmission of the VO_2 in Fig. 3.

Fig. 3 shows the spectrally expanded upon results from Fig. 2(c). As seen in Fig. 2(d), the overall fit for the impulse time of transition is 24 fs FWHM. Fig. 3(a) shows the time and frequency resolved change in transmission given by Eq. 1. The wavelength range between the solid colored lines are expanded upon in Fig. 3(b). The integrated signal between each lineout color in Fig. 3(a) corresponds to its equivalently colored curve in Fig. 3(b). The x's show the raw processed data given by Eq. 1, and the solid lines are the fit given by Eq. 2. We can see that for the regions outside the central wavelengths ($< 1800 \text{ nm}$, $> 1900 \text{ nm}$), the time of transmission remains relatively short (~ 20 fs) as seen by the slope of the blue and red lines respectively. On the contrary, for near the central wavelengths, black lines, we see that the time of transition is much longer (~ 35 fs). Spectrally resolving the transition times shows that the impulse for the transition indeed follows the pulse duration of the probe

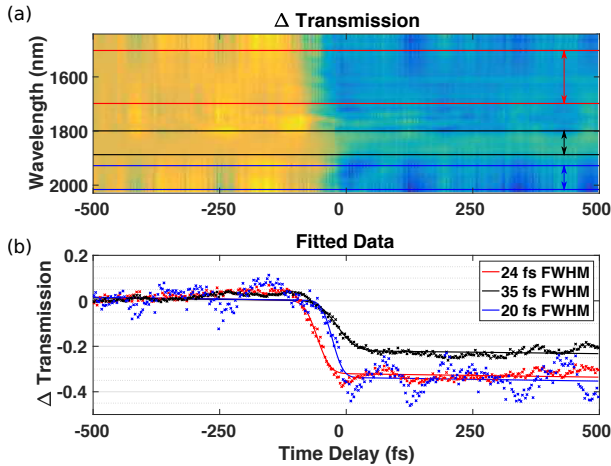


FIG. 3. 100 nm epitaxially grown VO_2 sample pumped with 80 mJ cm^{-2} . (a) This shows the time and frequency resolved change in transmission given by Eq. 1. The sum between the colored lines is fitted and plotted below. (b) Each color curve corresponds to the wavelength range between the same colored lines in the top graph. The x's show the raw processed data given by Eq. 1, and the solid lines are the fit given by Eq. 2.

pulse.

III.2. Change in transmission

We spectrally resolve the change in transmission of the probe as a function of the probe wavelength and the pump fluence, using the spectra collected from the slit based monochromator for this measurement. We calculate the change in transmission given by Eq. 1 at a delay time of $t = 1000 \text{ fs}$, using transmitted unpumped spectra through the VO_2 sample as the reference. By measuring the final change in transmission long after the pump, it will only depend on the pump fluence and probe wavelength. This means that a change in transmission of 0.6 corresponds to a transmission of 40%, with the other 60% either reflected or absorbed by the sample.

A saturation point in the overall change in transmission for the wavelengths probed is reached at about 60 mJ cm^{-2} , as seen in Fig. 4. For the wavelengths probed, this saturation point depends on the thickness of the VO_2 layer. With a 100 nm layer of epitaxial VO_2 the saturation point is at about 40% transmission (Fig. 4(a)).

The broadband probe allows spectral resolution in the wavelength dependence of the change in transmission, as seen in Fig. 4(a). The dashed line marks the 0.683 eV (1815 nm) band gap of the VO_2 , and the form of the absorption changes right around the band gap. We see a sharp increase followed by a sharp decrease in the change of transmission for photon energies just higher than the band gap. The observed results indicate an effect of the material near its band gap in the spectrally resolved transmission.

To better understand the change in transmission as a

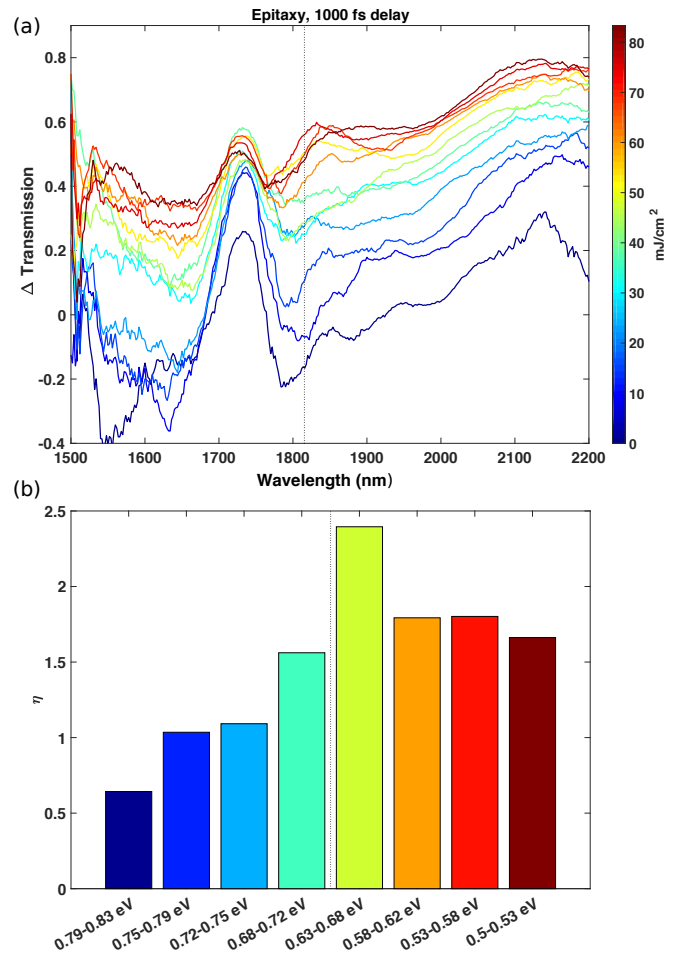


FIG. 4. Change in transmission for the epitaxial VO_2 sample. (a) Wavelength resolved change in transmission for 100 nm thick epitaxially grown VO_2 film, with a saturation point of $\sim 40\%$ transmission. The dotted vertical line corresponds to the 0.683 eV (1815 nm) band gap of the sample. (b) This shows the given η for above and below the band gap (denoted by the dashed black line) fitted from the log of the change in transmission as a function of the log of laser fluence.

function of laser fluence, we interpret the result as described in the framework of the lowest order perturbation theory²⁰. At the low intensities used to optically induce the phase transition in VO_2 , we are in the perturbative, multiphoton regime. Here, the electric field of the laser is not sufficiently large enough to modify the electric potential of the system to induce tunneling. Instead, an electron can absorb enough photons until it has enough energy to overcome the potential of the band gap of the material. In this regime the rate of electron emission is correlated to the number of photons, η , absorbed by the system as $J(I) \propto I^\eta$ ^{20,21}. This power law is used also to describe above threshold ionization (ATI) and above threshold photoemission (ATP) in other field-induced photoemission processes²². We can relate this to the change in transmission, by assuming that the change in transmission is proportional to the electron current emitted in above threshold processes (i.e. the number

of electrons that are freed to form holon-doublon pairs). Thus, we can calculate a correlation number, η , as a function of wavelength for the change in transmission of the VO₂.

By plotting the change in transmission as a function of laser fluence on a log scale, we extract the correlation value η above and below the band gap. We see that for photon energies less than the band gap (redder bars in Fig. 4(b), to the right of the dashed line), η is greater than 1 and for higher photon energies (bluer bars in Fig. 4(b), to the left of the dashed line), the extracted η is around 1. As η should correspond to the number of photons absorbed by the system, one would assume that for photon energies greater than the band gap, the η needed to trigger the phase transition would be 1, and subsequently for photon energies less than the band gap, the extracted η should be 2 or more. The fluctuations around the expected values are subject to further investigation.

IV. CONCLUSIONS

Using few-cycle infrared pulses, we are able to confirm that the phase transition in VO₂ is initiated by a

prompt creation of holon-doublon pairs. This is in good agreement with the instantaneous Mott insulator physics describing electron site hopping within Hubbard model. Using the spectrally resolved transmission as a function of pump fluence, we also observe an effect in the change in transmission from below to above the band gap. The observed instantaneous IMT of VO₂ will allow for a versatility in future applications that is unhindered by long structural timescales.

ACKNOWLEDGMENTS

We acknowledge NSERC, FRQNT, MESI, and CFI-MSI. VG was supported by the Air Force Office of Scientific Research under MURI, Award No. FA9550-16-1-0013. VW was supported by the Vanier Canada Graduate Scholarship. We thank Antoine Laramée for his technical contributions.

-
- ¹ D. Wegkamp and J. Stähler, *Prog. Surf. Sci.* **90**, 464 (2015).
² F. J. Morin, *Phys. Rev. Lett.* **3**, 34 (1959).
³ W. R. Roach and I. Balberg, *Solid State Commun.* **9**, 551 (1971).
⁴ N. F. Mott and L. Friedman, *Philos. Mag.* **30**, 389 (1974).
⁵ A. Zylbersztejn and N. F. Mott, *Phys. Rev. B* **11**, 4383 (1975).
⁶ A. Cavalleri, T. Dekorsy, H. H. W. Chong, J. C. Kieffer, and R. W. Schoenlein, *Phys. Rev. B* **70**, 161102(R) (2004).
⁷ C. Kübler, H. Ehrke, R. Huber, R. Lopez, A. Halabica, R. F. Haglund, and A. Leitenstorfer, *Phys. Rev. Lett.* **99**, 116401 (2007).
⁸ A. Pashkin, C. Kübler, H. Ehrke, R. Lopez, A. Halabica, R. F. Haglund, R. Huber, and A. Leitenstorfer, *Phys. Rev. B* **83**, 195120 (2011).
⁹ D. Wegkamp, M. Herzog, L. Xian, M. Gatti, P. Cudazzo, C. L. McGahan, R. E. Marvel, R. F. Haglund, A. Rubio, M. Wolf, and J. Stähler, *Phys. Rev. Lett.* **113**, 216401 (2014).
¹⁰ T. Oka, *Phys. Rev. B* **86**, 075148 (2012).
¹¹ B. Mayer, C. Schmidt, A. Grupp, J. Bühler, J. Oelmann, R. E. Marvel, R. F. Haglund, T. Oka, D. Brida, A. Leitenstorfer, and A. Pashkin, *Phys. Rev. B* **91**, 235113 (2015).
¹² V. R. Morrison, R. P. Chatelain, K. L. Tiwari, A. Hendaoui, A. Bruhács, M. Chaker, and B. J. Siwick, *Science* **346**, 455 (2014).
¹³ M. F. Jager, C. Ott, P. M. Kraus, C. J. Kaplan, W. Pouse, R. E. Marvel, R. F. Haglund, D. M. Neumark, and S. R. Leone, *PNAS* **114**, 9558 (2017).
¹⁴ R. M. Wentzcovitch, W. W. Schulz, and P. B. Allen, *Phys. Rev. Lett.* **72**, 3389 (1994).
¹⁵ S. Wall, L. Foglia, D. Wegkamp, K. Appavoo, J. Nag, R. F. Haglund, J. Stähler, and M. Wolf, *Phys. Rev. B* **87**, 115126 (2013).
¹⁶ N. Émond, A. Hendaoui, and M. Chaker, *Appl. Phys. Lett.* **107**, 143507 (2015).
¹⁷ Y. Zhao, J. Hwan Lee, Y. Zhu, M. Nazari, C. Chen, H. Wang, A. Bernussi, M. Holtz, and Z. Fan, *J. App. Phys.* **111**, 053533 (2012).
¹⁸ B. E. Schmidt, P. Béjot, M. Giguère, A. D. Shiner, C. Trallero-Herrero, É. Bisson, J. Kasparian, J. P. Wolf, D. M. Villeneuve, J. C. Kieffer, P. B. Corkum, and F. Légaré, *Appl. Phys. Lett.* **96**, 121109 (2010).
¹⁹ R. Trebino, K. W. DeLong, D. N. Fittinghoff, J. N. Sweetser, M. A. Krumbügel, B. A. Richman, and D. J. Kane, *Rev. Sci. Inst.* **68**, 3277 (1997).
²⁰ C. Joachain, N. Kylstra, and R. Potvliege, *Atoms in Intense Laser Fields* (Cambridge University Press, Cambridge, 2012).
²¹ L. Keldysh, *Soviet Physics JETP* **20**, 1307 (1965).
²² M. Bionta, B. Chalopin, J. Champeaux, S. Faure, A. Masseboeuf, P. Moretto-Capelle, and B. Chatel, *J. Mod. Opt.* **61**, 833 (2014).